Electronic Research Archive

http://www.aimspress.com/journal/era

ERA, 34(4): 2433–2461.
DOI: 10.3934/era.2026112
Received: 29 December 2025
Revised: 15 February 2026
Accepted: 28 February 2026
Published: 23 March 2026

Research article

Dynamical analysis of impulsive insulin delivery in a glucose-insulin system with insulin-degrading enzyme effects

Zhongyuan Zhang[1], **Qiqi Zheng**[1] **and Mingzhan Huang**[1,2,*]

[1] School of Mathematics and Statistics, Xinyang Normal University, Xinyang 464000, China

[2] Henan Provincial Center for Applied Mathematics, Xinyang Normal University, Xinyang 464000, China

* **Correspondence:** Email: huangmingzhan@163.com.

Abstract: This paper investigated impulsive insulin therapy within an extended glucose-insulin regulatory system that included insulin-degrading enzyme dynamics. Two treatment modes were examined: periodic delivery and state-dependent feedback. For the periodic model, we established solution positivity and boundedness, proved the global asymptotic stability of a unique positive periodic solution for type I diabetes, and derived permanence bounds along with a safe dosing region for type II diabetes. For the state-dependent model, under mild conditions, we demonstrated the existence and global orbital asymptotic stability of a unique order-1 periodic orbit within a physiologically relevant glucose range. Numerical simulations supported the theoretical results and illustrated how the choice of dosing period, bolus size, and threshold level influenced long-term glucose control. The results provided a unified theoretical framework for comparing and optimizing impulsive insulin therapies.

Keywords: glucose-insulin model; impulsive injection; periodic solution; stability

1. Introduction

Hyperglycaemia remains a central hallmark of diabetes and a major risk factor for both acute and chronic complications [1]. Modern insulin therapies aim not only to reduce mean glucose levels but also to suppress excessive excursions while avoiding hypoglycaemia. This clinical goal naturally leads to hybrid dynamical descriptions: glucose-insulin interactions evolve continuously in time, whereas therapeutic interventions (e.g., bolus delivery through pumps or controller-triggered injections in an artificial pancreas) occur as discrete events. Impulsive differential equation models and related semi-continuous dynamical systems therefore provide a mathematically transparent and physiologically interpretable framework for studying treatment-induced glucose regulation [2, 3].

Recent advances in glucose-insulin modeling have incorporated delay differential equations [4], fractional-order dynamics [5], and stochastic effects [6, 7] to capture more complex physiological phenomena. As a supplement to these methods, the impulsive delivery mechanisms in deterministic environments establish a baseline for integrating delays or randomness extensions. A considerable literature has investigated glucose-insulin regulation under impulsive insulin delivery. Classical two-compartment impulsive differential equation models represent insulin pump therapy via periodic bolus injections with fixed dose and fixed period, and represent artificial pancreas therapy via state-dependent (threshold-triggered) injections motivated by feedback from continuous glucose monitoring [8–10]. These models have clarified mechanisms for the emergence of periodic responses and have enabled stability analysis through Poincaré maps and hybrid dynamical techniques. However, some modeling limitations remain important for therapy-oriented studies. In particular, physiological descriptions of insulin handling are often oversimplified in ways that become non-negligible in the clinically relevant regime. A common simplification is to model insulin degradation (clearance) as a linear loss. While linear clearance is analytically convenient and reasonable at low insulin levels, clinical and physiological evidence indicates a finite capacity of insulin removal pathways. Consequently, saturation-like behavior can arise in effective clearance rates under frequent boluses or high insulin concentrations [11–13]. Neglecting this nonlinearity may bias predictions of insulin dynamics and pattern stability, and can therefore lead to misleading assessments of a strategy's long-term safety and efficacy [14, 15].

Another mechanism that has attracted increasing attention is the role of insulin-degrading enzyme (IDE) in insulin metabolism and its association with insulin dysregulation in metabolic disorders. IDE participates in insulin clearance and has been implicated in impaired insulin action and related pathological states [16–18]. Thus, the effective generation and availability of insulin in vivo may be influenced not only by glucose-stimulated secretion but also by the metabolic environment associated with insulin handling [19–21]. Nevertheless, many therapy-oriented models still treat glucose-stimulated insulin production as a function of glucose alone, without incorporating an IDE-related modulation factor. This omission may weaken a model's capability to capture clinically observed variability across patients or disease stages, and may limit the interpretability of simulation-based therapy comparisons [21, 22]. In particular, the combined effects of IDE-mediated modulation and saturable clearance on the qualitative behavior of impulsive treatment strategies have not been systematically analyzed in a unified framework.

Motivated by these considerations, we propose two mechanism-enriched models for hyperglycaemia treatment in this work. The models incorporate (i) an IDE-modulated glucose-stimulated insulin production term, which links effective insulin generation to both glycaemic levels and the metabolic environment for insulin handling; and (ii) a Michaelis–Menten type insulin degradation term that captures saturation at higher concentrations. On this shared physiological kernel, we formulate two treatment modules aligned with clinical practice: an open-loop model with periodic impulsive dosing (simulating insulin pump therapy), and a closed-loop model with state-dependent impulsive dosing (representing an artificial pancreas strategy with an insulin safety constraint). The resulting systems are hybrid dynamical models consisting of continuous-time glucose–insulin kinetics coupled with discrete impulsive actions.

The incorporation of IDE-modulated insulin production and saturable degradation yields several novel qualitative insights. First, it reveals that under frequent bolus delivery, the saturation of insulin

clearance (Michaelis-Menten kinetics) may significantly alter the effective insulin dynamics, leading to a nonlinear dose-response relationship. Second, the IDE modulation factor links insulin effectiveness to the metabolic environment, enabling the model to capture patient-specific variability in insulin handling. These features advance current theory by providing a more physiologically grounded framework for analyzing impulsive insulin therapies, and they offer practical guidance for tuning dosing parameters to achieve desired glycemic outcomes while avoiding hypoglycemia.

The remainder of this paper is organized as follows. Section 2 introduces the model formulation and details the underlying biological assumptions. Section 3 presents the dynamical analysis of both the periodic and state-dependent impulsive regulatory systems. Section 4 provides numerical simulations to validate the theoretical results and examine the impact of pulse parameters on glucose control. Finally, Section 5 contains brief concluding remarks.

2. Model formulation

We denote $G(t)$ as the blood glucose level and $I(t)$ as the insulin level at time t. Glucose dynamics are governed by four components: a basal input $G_{\text{in}} > 0$, an insulin-independent utilization term $\sigma_2 G(t)$ ($\sigma_2 > 0$), a constant term b for net endogenous glucose production and other baseline effects, and an insulin-dependent uptake term

$$H(I) = c + \frac{mI}{n + I}, \qquad c, m, n > 0.$$

This term follows the framework of treatment-oriented impulsive insulin delivery models for glucose-insulin regulation [8,23,24], where c denotes basal insulin effectiveness and $\frac{mI}{n+I}$ describes the saturating effect of insulin on glucose uptake.

The constant glucose influx G_{in} represents the average rate of glucose entry from hepatic production and dietary intake under fasting conditions, a standard simplification in glucose-insulin modeling [8, 23, 24]. The constant term b corresponds to hepatic glucose production (HGP). In healthy individuals, HGP is regulated by insulin; however, for types 1 and 2 diabetic patients, little or no insulin is secreted from β-cells and exogenous insulin is delivered subcutaneously, making the direct control of HGP by insulin less significant. Therefore, following [24], we treat HGP as a constant rate $b > 0$.

For the insulin dynamics, glucose-stimulated insulin production is modeled by

$$F(G) = \frac{\sigma_1 G^2}{\alpha_1^2 + G^2}, \qquad \sigma_1, \alpha_1 > 0.$$

Motivated by IDE-related glucose–insulin modeling [21], we further modulate the effective production/availability by

$$\Phi(I) = \frac{k_0 I}{e^{c_1 I} - 1}, \qquad k_0, c_1 > 0,$$

with the continuous extension $\Phi(0) \triangleq \lim_{I \to 0^+} \Phi(I) = k_0/c_1$. The function $\Phi(I)$ is positive and strictly decreasing, reflecting reduced relative enhancement of insulin action when IDE activity is high (i.e., when insulin levels are elevated). The parameter k_0 scales the maximal modulation, while c_1 controls the sensitivity to insulin. This formulation captures the feedback between insulin concentration and its own degradation, a feature absent in traditional models that assume linear clearance.

Moreover, to capture saturation of insulin removal capacity, particularly relevant under frequent bolus delivery, we adopt a Michaelis-Menten clearance term

$$\Psi(I) = \frac{D_1 I}{D_2 + I}, \qquad D_1, D_2 > 0,$$

which is more realistic than purely linear degradation in high-insulin regimes [12, 13, 25].

With these components, we propose two treatment models sharing the same continuous kernel but differing in impulsive dosing mechanisms. For periodic impulsive insulin delivery (pump therapy), the impulse instants are prescribed by the periodic schedule

$$\mathcal{T}_p \triangleq \{t_k = kp : \ k \in \mathbb{Z}^+\},$$

and a bolus of size ϱ is administered at every $t_k \in \mathcal{T}_p$. Then, the full system is

$$\begin{cases} \left.\begin{aligned} \frac{dG(t)}{dt} &= G_{\text{in}} - \sigma_2 G(t) - aG(t)H(I(t)) + b, \\ \frac{dI(t)}{dt} &= F(G(t)) \cdot \Phi(I(t)) - \Psi(I(t)), \end{aligned}\right\} & t \in (0,\infty) \setminus \mathcal{T}_p, \\ \left.\begin{aligned} G(t^+) &= G(t), \\ I(t^+) &= I(t) + \varrho, \end{aligned}\right\} & t \in \mathcal{T}_p. \end{cases} \tag{2.1}$$

This model idealizes pump bolus injections as instantaneous increases in I, and is consistent with classical impulsive pump-therapy formulations.

For state-dependent impulsive insulin delivery (artificial pancreas), insulin is injected only when the glucose level reaches the prescribed threshold $G_C > 0$ and the insulin level does not exceed the safety threshold $I_P > 0$. Define the triggering (guard) manifold

$$\Gamma = \{(G, I) : \ G = G_C, \ I \le I_P\}.$$

Starting from (G_0, I_0), the impulse instants $\mathcal{T}_s \triangleq \{t_i\}_{i\ge 1}$ are generated by the trajectory as the successive first hitting times of Γ, namely,

$$t_i = \inf\{t > t_{i-1} : \ (G(t), I(t)) \in \Gamma\}, \qquad t_0 = 0.$$

At each $t_i \in \mathcal{T}_s$ an insulin bolus of size ϱ is applied, while no impulses occur for $t \notin \mathcal{T}_s$. The full state-dependent impulsive system is written as

$$\begin{cases} \left.\begin{aligned} \frac{dG(t)}{dt} &= G_{\text{in}} - \sigma_2 G(t) - aG(t)H(I(t)) + b, \\ \frac{dI(t)}{dt} &= F(G(t)) \cdot \Phi(I(t)) - \Psi(I(t)), \end{aligned}\right\} & t \in (0,\infty) \setminus \mathcal{T}_s, \\ \left.\begin{aligned} G(t_i^+) &= G(t_i), \\ I(t_i^+) &= I(t_i) + \varrho, \end{aligned}\right\} & t = t_i \in \mathcal{T}_s \ \text{(equivalently } (G(t_i), I(t_i)) \in \Gamma), \end{cases} \tag{2.2}$$

where the initial values satisfy $G(0) = G_0 \le G_C$ and $I(0) = I_0 > 0$. The critical value I_P is determined by the intersection of the nullcline $G'(t) = 0$ and the line $G = G_C$ in the (G, I)-plane. In particular, along $G = G_C$ one has $dG(t)/dt < 0$ whenever $I > I_P$, which justifies inhibiting further boluses when insulin is already high and mitigates over-delivery.

This event-triggered rule reflects the artificial pancreas design philosophy "inject when glucose is high, but avoid stacking insulin when insulin is already high", which aligns with threshold-based state-feedback impulsive therapy models [24, 26].

All parameter values are listed in Table 1 and are adapted from prior studies. For a detailed discussion on linking model equations to biological mechanisms, we refer to the recent work [27].

Models (2.1) and (2.2) share identical continuous dynamics, but differ fundamentally in their impulsive delivery mechanisms. Model (2.1) employs periodic impulses at fixed intervals p, representing open-loop insulin pump therapy, while model (2.2) employs state-dependent impulses triggered only when glucose reaches threshold G_C and insulin is below safety limit I_P, mimicking a closed-loop artificial pancreas. Thus, the two models capture distinct therapeutic paradigms and provide complementary insights into impulsive insulin delivery.

Table 1. Summary of variables and parameters.

Symbol	Description	Unit
G	Blood glucose concentration	mg/dL
I	Plasma insulin concentration	mU/L
G_{in}	Basal glucose influx	mg/min
σ_2	Insulin-independent glucose utilization rate	min^{-1}
a	Insulin sensitivity factor	mg^{-1}
b	Net endogenous glucose production	mg
c	Basal insulin effectiveness	mg/min
m	Maximal insulin-dependent glucose uptake	mg/min
n	Half-saturation constant for insulin-dependent uptake	mg
σ_1	Maximal glucose-stimulated insulin secretion rate	mU/min
α_1	Half-saturation constant for glucose-stimulated secretion	mg
k_0	IDE modulation scale	min^{-1}
c_1	IDE sensitivity parameter	-
D_1	Maximum insulin degradation rate	min^{-1}
D_2	Half-saturation constant for insulin degradation	min^{-1}
p	Dosing period (pump therapy)	min
ϱ	Bolus insulin dose	mU
G_C	Glucose threshold for state-dependent injection	mg/dL
I_P	Insulin safety limit for injection	mU/L

3. Dynamical analysis of the treatment systems

In this section, we carry out a rigorous dynamical analysis for the two impulsive treatment systems proposed in Section 2.

3.1. Dynamics of the periodic impulsive regulatory system

In this subsection, we analyze system (2.1), which represents periodic bolus delivery under pump therapy. We first establish well-posedness of the impulsive system and derive basic qualitative properties such as positivity and boundedness of solutions.

Let $x(t) = (G(t), I(t))^T$ and rewrite system (2.1) in the standard impulsive form

$$x'(t) = f(x(t)), \quad t \neq t_k, \qquad x(t_k^+) = x(t_k) + J, \quad t_k = kp,\ k \in \mathbb{Z}^+,$$

where $f = (f_G, f_I)^T$ is given by the righthand sides of the differential equations in (2.1) and $J = (0, \varrho)^T$. By defining the continuous extension $\Phi(0) = k_0/c_1$, the map f is continuous on $\mathbb{R}^2_+$ and locally Lipschitz with respect to x on $\mathbb{R}^2_+$. Moreover, the impulse-time sequence $\{t_k\}$ is strictly increasing and satisfies $t_k \to \infty$ as $k \to \infty$, while the impulse operator $x \mapsto x + J$ is continuous. Therefore, for any initial condition $x(0) = (G_0, I_0)^T \in \mathbb{R}^2_+$, system (2.1) admits a unique solution in the sense of impulsive differential equations on each interval $[0, t_k]$, and, hence, a unique global solution on $[0, \infty)$. This follows directly from the classical existence and uniqueness theory for impulsive differential equations [28, 29].

In the following, we show that solutions of system (2.1) with nonnegative initial values remain nonnegative and bounded for all $t \geq 0$.

Proposition 1. *Assume $x(0) = (G_0, I_0)^T \in \mathbb{R}^2_+$. Then, the solution $(G(t), I(t))$ of system (2.1) satisfies $G(t) \geq 0$, $I(t) \geq 0$ for all $t \geq 0$.*

Proof. For $t \notin \mathcal{T}_p$, from the first equation in (2.1), we get

$$G'(t)|_{G=0} = G_{\text{in}} - \sigma_2 \cdot 0 - a \cdot 0 \cdot H(I(t)) + b = G_{\text{in}} + b > 0,$$

hence, $G(t)$ cannot cross from $G \geq 0$ into $G < 0$.

Next, using the continuous extension $\Phi(0) = k_0/c_1$ and $\Psi(0) = 0$, we have

$$I'(t)|_{I=0} = F(G(t))\,\Phi(0) - \Psi(0) = F(G(t))\frac{k_0}{c_1} \geq 0,$$

so $I(t)$ cannot cross from $I \geq 0$ into $I < 0$.

At each impulse instant $t = t_k \in \mathcal{T}_p$, we have $G(t_k^+) = G(t_k)$ and $I(t_k^+) = I(t_k) + \varrho$ with $\varrho > 0$, which preserve nonnegativity. Therefore, $(G(t), I(t)) \in \mathbb{R}^2_+$ for all $t \geq 0$.

To facilitate the boundedness and long-term behavior analysis for system (2.1), we shall compare the insulin dynamics with an auxiliary impulsive equation whose explicit solutions can be expressed via the Lambert W function. For completeness, we first recall the definition of the Lambert W function and then state a technical lemma that will be used later.

The Lambert W function W is defined as the (multivalued) inverse of the mapping $z \mapsto ze^z$, and, hence, satisfies

$$W(z)\exp(W(z)) = z.$$

Lemma 1. *Consider the following piecewise impulsive system*

$$\begin{cases} u'(t) = a_1 - \dfrac{b_1 u(t)}{c_2 + u(t)}, & t \neq kp, \\ u(t^+) = u(t) + \varrho, & t = kp, \\ u(0^+) = u_0 > 0, \end{cases} \tag{3.1}$$

where $k \in \mathbb{Z}^+$ and $a_1, b_1, c_2, \varrho, p$ are nonnegative constants with $c_2 > 0$ and $p > 0$.

(i) If $a_1 \geq b_1$, then every solution of (3.1) *is monotonically increasing in t and unbounded.*

(ii) If $0 \leq a_1 < b_1$ and $\varrho < (b_1 - a_1)p$, then (3.1) *admits a unique positive p-periodic solution $\tilde{u}(t)$, which is globally asymptotically stable and satisfies*

$$\left|u(t) - \tilde{u}(t)\right| \to 0, \qquad t \to +\infty.$$

Moreover, the periodic solution admits the explicit representation

$$\tilde{u}(t) = \frac{b_1 c_2}{b_1 - a_1} W(\Theta(\tilde{u}(0^+), t)) + \frac{a_1 c_2}{b_1 - a_1}, \quad t \in (kp^+, (k+1)p],\ k \in \mathbb{Z}^+, \tag{3.2}$$

where

$$\Theta(\tilde{u}(0^+), t) = \frac{b_1 - a_1}{b_1 c_2}\Big(\tilde{u}(0^+) - \frac{a_1 c_2}{b_1 - a_1}\Big) \exp\left(\frac{b_1 - a_1}{b_1 c_2}\Big(\tilde{u}(0^+) - \frac{a_1 c_2}{b_1 - a_1} - (b_1 - a_1)(t - kp)\Big)\right). \tag{3.3}$$

The initial value $\tilde{u}(0^+)$ is determined by the periodicity condition and is given by

$$\tilde{u}(0^+) = \frac{\varrho}{1 - M} + \frac{a_1 c_2}{b_1 - a_1}, \tag{3.4}$$

where

$$M = \exp\left\{\frac{(b_1 - a_1)\left[\varrho - (b_1 - a_1)p\right]}{b_1 c_2}\right\}.$$

(iii) If $a_1 = 0$ and $\varrho < b_1 p$, then (3.1) *admits a globally stable p-periodic solution*

$$\tilde{u}_1(t) = c_2 W\left(\frac{\tilde{u}_1(0^+)}{c_2} \exp\left(\frac{\tilde{u}_1(0^+) - b_1(t - kp)}{c_2}\right)\right), \quad t \in (kp^+, (k+1)p], \tag{3.5}$$

with

$$\tilde{u}_1(0^+) = \frac{\varrho}{1 - \exp\Big(\frac{\varrho - b_1 p}{c_2}\Big)}. \tag{3.6}$$

Proof. The proof of Lemma 1 is deferred to Appendix A.

Proposition 2. *Let $(G(t), I(t))$ be the solution of system* (2.1) *with initial value $x_0 = (G_0, I_0) \in \mathbb{R}^2_+$. If $0 \leq \sigma_1 \frac{k_0}{c_1} < D_1$ and $\varrho < \Big(D_1 - \sigma_1 \frac{k_0}{c_1}\Big)p$, then for all $t \geq 0$,*

$$0 \leq G(t) \leq \max\Big\{G_0,\ \frac{G_{\text{in}} + b}{\sigma_2 + ac}\Big\} \triangleq G^U, \qquad 0 \leq I(t) \leq \max\{I_0, I_M^*\} \triangleq I^U,$$

where I_M^* is defined in (3.10).

Proof. By Proposition 1, $G(t), I(t) \geq 0$ for all $t \geq 0$. Since $H(I) = c + \dfrac{mI}{n + I} \geq c$ for $I \geq 0$, we obtain

$$G'(t) = G_{\text{in}} - \sigma_2 G(t) - aG(t)H(I(t)) + b \leq G_{\text{in}} + b - (\sigma_2 + ac)G(t),$$

for $t \neq t_k$. As G does not jump at t_k, the comparison principle yields

$$0 \leq G(t) \leq \max\Big\{G_0,\ \frac{G_{\text{in}} + b}{\sigma_2 + ac}\Big\} = G^U, \qquad t \geq 0.$$

For $t \neq t_k$, the insulin equation in (2.1) satisfies

$$I'(t) = F(G(t))\,\Phi(I(t)) - \Psi(I(t)) \leq \sigma_1 \frac{k_0}{c_1} - \frac{D_1 I(t)}{D_2 + I(t)}.$$

At each impulse time $t = t_k = kp$, $I(t_k^+) = I(t_k) + \varrho$.

Consider the auxiliary impulsive system

$$\begin{cases} I_M'(t) = \sigma_1 \frac{k_0}{c_1} - \dfrac{D_1 I_M(t)}{D_2 + I_M(t)}, & t \neq kp, \\ I_M(t^+) = I_M(t) + \varrho, & t = kp, \\ I_M(0^+) = I_0. \end{cases} \tag{3.7}$$

System (3.7) is exactly of the form (3.1) with $a_1 = \sigma_1 \frac{k_0}{c_1}$, $b_1 = D_1$, and $c_2 = D_2$. By the comparison principle for impulsive systems, we have

$$I(t) \leq I_M(t), \qquad \forall\, t \geq 0. \tag{3.8}$$

Under the conditions $0 \leq \sigma_1 \frac{k_0}{c_1} < D_1$ and $\varrho < \left(D_1 - \sigma_1 \frac{k_0}{c_1}\right)p$, Lemma 1(ii) implies that system (3.7) admits a unique globally asymptotically stable positive p-periodic solution

$$\tilde{I}_M(t) = \frac{D_1 D_2}{D_1 - \sigma_1 \frac{k_0}{c_1}} W(\Theta(\tilde{I}_M(0^+), t)) + \frac{\sigma_1 k_0 D_2}{c_1 D_1 - \sigma_1 k_0},\ t \in (kp^+, (k+1)p], \tag{3.9}$$

with

$$I_M^* \triangleq \tilde{I}_M(0^+) = \frac{\varrho}{1 - M_1} + \frac{\sigma_1 k_0 D_2}{c_1 D_1 - \sigma_1 k_0},\ M_1 = \exp\left\{ \frac{(D_1 - \sigma_1 \frac{k_0}{c_1})[\varrho - (D_1 - \sigma_1 \frac{k_0}{c_1})p]}{D_1 D_2} \right\}. \tag{3.10}$$

As shown in the proof of Lemma 1 in Appendix A, the associated stroboscopic map $P(I_M(kp^+)) = I_M((k+1)p^+)$ is strictly increasing with $0 < P' < 1$ and has the unique fixed point I_M^*. Consequently, the post-impulse sequence $I_M(kp^+)$ is monotone and satisfies

$$\min\{I_0, I_M^*\} \leq I_M(kp^+) \leq \max\{I_0, I_M^*\}, \qquad k = 0, 1, 2, \ldots.$$

Moreover, on each interval $(kp, (k+1)p]$, the solution $I_M(t)$ is monotone in t and never exceeds $\max\{I_M(kp^+), I_M^\Delta\}$, where $I_M^\Delta = \dfrac{\sigma_1 k_0 D_2}{c_1 D_1 - \sigma_1 k_0}$ is the unique equilibrium of the continuous flow. Since $I_M^* > I_M^\Delta$, we infer that $0 \leq I_M(t) \leq \max\{I_0, I_M^*\}$ for all $t \geq 0$.

Using the comparison estimate (3.8), we finally obtain

$$0 \leq I(t) \leq I_M(t) \leq \max\{I_0, I_M^*\} = I^U, \qquad \forall\, t \geq 0.$$

This completes the proof.

Next, we examine the existence of positive periodic solutions of system (2.1). To highlight the role of exogenous insulin delivery, we first consider the case of type I diabetes (T1DM), in which endogenous insulin secretion is absent, that is,

$$F(G) \equiv 0 \quad \text{(equivalent to } \sigma_1 = 0\text{)}.$$

In this case, the insulin dynamics are governed solely by pump boluses and saturable degradation. We claim that, under the above dosing condition, the reduced system admits a positive p-periodic solution, corresponding to the steady response to the prescribed pump therapy.

Before establishing the attractivity of the periodic solution, we first verify the well-posedness of system (2.1). By Proposition 1, any solution with initial condition $(G_0, I_0) \in \mathbb{R}^2_+$ remains nonnegative for all $t \geq 0$. Moreover, following the classical existence and uniqueness theory for impulsive differential equations [28, 29], the solution exists uniquely on each interval $[0, t_k]$ and, hence, on the whole interval $[0, \infty)$. This guarantees that the solution is globally defined and remains in $\mathbb{R}^2_+$, which is a prerequisite for the subsequent attractivity analysis (see also [30, 31] for similar treatments in related models).

Theorem 1. *Assume that $\sigma_1 = 0$ and $\varrho < D_1 p$. Then, system* (2.1) *admits a unique positive p-periodic solution $(\tilde{G}(t), \tilde{I}(t))$ which is globally asymptotically stable.*

Proof. When $\sigma_1 = 0$, the insulin equation in system (2.1) reduces to

$$\begin{cases} \frac{dI(t)}{dt} = -\frac{D_1 I(t)}{D_2 + I(t)}, & t \neq kp, \\ I(t^+) = I(t) + \varrho, & t = kp,\ k \in \mathbb{Z}^+. \end{cases} \tag{3.11}$$

Under condition $\varrho < D_1 p$, Lemma 1(iii) implies that the insulin subsystem (3.11) admits a globally asymptotically stable p-periodic solution

$$\tilde{I}(t) = D_2 W\left(\frac{\tilde{I}(0^+)}{D_2} \exp\left(\frac{\tilde{I}(0^+) - D_1(t - kp)}{D_2}\right)\right),\ t \in (kp, (k+1)p], \tag{3.12}$$

with $\tilde{I}(0^+) = \frac{\varrho}{1 - \exp\left(\frac{\varrho - D_1 p}{D_2}\right)}$. In particular, any solution of system (2.1) satisfies $\lim_{t\to\infty} I(t) = \tilde{I}(t)$.

Substituting $\tilde{I}(t)$ into the glucose equation yields

$$\frac{dG(t)}{dt} = G_{\text{in}} - \sigma_2 G(t) - aG(t)H(\tilde{I}(t)) + b = r_1 - \zeta_{\tilde{I}}(t)G(t), \quad t \neq kp, \tag{3.13}$$

where $r_1 \triangleq G_{\text{in}} + b > 0$ and $\zeta_{\tilde{I}}(t) \triangleq \sigma_2 + aH(\tilde{I}(t)) \geq \sigma_2 + ac > 0$.

Since G does not jump at $t = kp$ and $\tilde{I}(t)$ is p-periodic, $\zeta_{\tilde{I}}(t)$ is continuous and p-periodic. For any $G(0) = G_0 \geq 0$, the solution of (3.13) can be written explicitly as

$$G(t; G_0) = \exp\Big(-\int_0^t \zeta_{\tilde{I}}(s)\,ds\Big)\Big(G_0 + r_1 \int_0^t \exp\Big(\int_0^\xi \zeta_{\tilde{I}}(s)\,ds\Big)\,d\xi\Big), \qquad t \geq 0.$$

Define the stroboscopic map $P_G : \mathbb{R}_+ \to \mathbb{R}_+$ by

$$P_G(G_0) \triangleq G(p; G_0).$$

Hence,

$$P_G(G_0) = \gamma G_0 + \kappa_0,$$

where

$$\gamma = \exp\Big(-\int_0^p \zeta_{\tilde{I}}(s)\,ds\Big) \in (0, 1),\ \kappa_0 = \exp\Big(-\int_0^p \zeta_{\tilde{I}}(s)\,ds\Big) \int_0^p \exp\Big(\int_0^\xi \zeta_{\tilde{I}}(s)\,ds\Big)\,r\,d\xi > 0.$$

In particular, for any $G_1, G_2 \in \mathbb{R}_+$,

$$|P_G(G_1) - P_G(G_2)| = \gamma\,|G_1 - G_2|,$$

so P_G is a strict contraction on the complete metric space $(\mathbb{R}_+, |\cdot|)$. By the Banach fixed point theorem, there exists a unique $\tilde{G}^* \in \mathbb{R}_+$ such that $P_G(\tilde{G}^*) = \tilde{G}^*$. Moreover, since $\kappa_0 > 0$ and $\gamma \in (0,1)$, we have

$$\tilde{G}^* = P_G(\tilde{G}^*) = \gamma\tilde{G}^* + \kappa_0 = \frac{\kappa_0}{1-\gamma} > 0,$$

so the fixed point is in fact strictly positive. Denoting $\tilde{G}(0) \triangleq \tilde{G}^*$ and letting

$$\tilde{G}(t) = \exp\Big(-\int_0^{t-kp} \zeta_{\tilde{I}}(s)\,ds\Big)\Big(\tilde{G}^* + r_1\int_0^{t-kp} \exp\Big(\int_0^{\xi} \zeta_{\tilde{I}}(s)\,ds\Big)\,d\xi\Big),\ t \in (kp,(k+1)p], \tag{3.14}$$

we know that $\tilde{G}(t)$ is the unique positive p-periodic solution of (3.13). Thus, $(\tilde{G}(t), \tilde{I}(t))$ is the unique positive p-periodic solution of system (2.1).

Furthermore, the contraction property of P_G implies that for any $G_0 \geq 0$, $G(kp; G_0) \to \tilde{G}^*$ as $k \to \infty$, and then we obtain, by continuity,

$$G(t; G_0) \to \tilde{G}(t) \quad \text{as} \quad t \to \infty.$$

Note that the associated stroboscopic map P_G has a unique fixed point with multiplier $\gamma \in (0,1)$, which ensures local (exponential) stability of the periodic orbit. In addition, the periodic solution $(\tilde{G}(t), \tilde{I}(t))$ attracts all solutions of system (2.1) in $\mathbb{R}^2_+$ and is therefore globally asymptotically stable. This completes the proof.

Remark 1. *The global asymptotic stability in Theorem 1 means that the periodic solution* $(\tilde{G}(t), \tilde{I}(t))$ *attracts all solutions starting from any initial condition in* $\mathbb{R}^2_+$*. Thus, the domain of attraction is the entire nonnegative quadrant* $\mathbb{R}^2_+$*.*

We now turn to the case of type II diabetes (T2DM), where endogenous insulin secretion remains active, that is, $\sigma_1 > 0$ (equivalently, $F(G) \not\equiv 0$). Building on the positivity and uniform upper bounds established above, we next show that system (2.1) is permanent.

Theorem 2. *Assume* $0 < \sigma_1\frac{k_0}{c_1} < D_1$ *and* $\varrho < \Big(D_1 - \sigma_1\frac{k_0}{c_1}\Big)p$*. Then, system* (2.1) *is permanent in the sense that all solutions with* $(G_0, I_0) \in \mathbb{R}^2_+$ *eventually enter and remain in the compact rectangle*

$$\mathcal{R} \triangleq [G_m, G_M] \times [\tilde{I}_{\mathrm{m}}(p), \tilde{I}_{\mathrm{M}}(0^+)] \subset \mathbb{R}^2_+,$$

where $G_m, G_M > 0$ *and* $\tilde{I}_{\mathrm{m}}(p), \tilde{I}_{\mathrm{M}}(0^+) > 0$ *are as defined below.*

Proof. According to the insulin equation in system (2.1), for $t \neq kp$ we have

$$-\frac{D_1 I(t)}{D_2 + I(t)} \ \leq\ I'(t) = F(G(t))\,\Phi(I(t)) - \Psi(I(t)) \ \leq\ \sigma_1\frac{k_0}{c_1} - \frac{D_1 I(t)}{D_2 + I(t)}, \tag{3.15}$$

while $I(kp^+) = I(kp) + \varrho$. Here we used that $0 \leq F(G(t)) \leq \sigma_1$ and $0 \leq \Phi(I(t)) \leq k_0/c_1$.

Consider the auxiliary impulsive systems

$$\begin{cases} I'_{\mathrm{m}}(t) = -\dfrac{D_1 I_{\mathrm{m}}(t)}{D_2 + I_{\mathrm{m}}(t)}, & t \neq kp, \\ I_{\mathrm{m}}(t^+) = I_{\mathrm{m}}(t) + \varrho, & t = kp, \\ I_{\mathrm{m}}(0^+) = I_0, \end{cases} \tag{3.16}$$

and

$$\begin{cases} I'_{\mathrm{M}}(t) = \sigma_1 \frac{k_0}{c_1} - \dfrac{D_1 I_{\mathrm{M}}(t)}{D_2 + I_{\mathrm{M}}(t)}, & t \neq kp, \\ I_{\mathrm{M}}(t^+) = I_{\mathrm{M}}(t) + \varrho, & t = kp, \\ I_{\mathrm{M}}(0^+) = I_0. \end{cases} \tag{3.17}$$

The inequalities in (3.15), together with the identical jump rule at $t = kp$, enable us to apply the comparison principle for impulsive equations, leading to the conclusion that

$$I_{\mathrm{m}}(t) \leq I(t) \leq I_{\mathrm{M}}(t), \qquad t \geq 0.$$

Under the conditions $0 < \sigma_1 \frac{k_0}{c_1} < D_1$ and $\varrho < \left(D_1 - \sigma_1 \frac{k_0}{c_1}\right)p$, Lemma 1 guarantees that $I_{\mathrm{m}}(t)$ and $I_{\mathrm{M}}(t)$ converge to positive p-periodic solutions $\tilde{I}_{\mathrm{m}}(t)$ and $\tilde{I}_{\mathrm{M}}(t)$, respectively. In particular, $I_{\mathrm{m}}(t) \to \tilde{I}_{\mathrm{m}}(t)$ and $I_{\mathrm{M}}(t) \to \tilde{I}_{\mathrm{M}}(t)$ as $t \to \infty$, where $\tilde{I}_{\mathrm{m}}(t)$ coincides with the periodic solution $\tilde{I}(t)$ given in (3.12), and $\tilde{I}_{\mathrm{M}}(t)$ is given in (3.9).

Since $I_{\mathrm{m}}(t) \leq I(t) \leq I_{\mathrm{M}}(t)$ for all $t \geq 0$, we obtain

$$0 < \min_{t\in[0,p]} \tilde{I}_{\mathrm{m}}(t) = \liminf_{t\to\infty} I_{\mathrm{m}}(t) \leq \liminf_{t\to\infty} I(t) \leq \limsup_{t\to\infty} I(t) \leq \limsup_{t\to\infty} I_{\mathrm{M}}(t) = \max_{t\in[0,p]} \tilde{I}_{\mathrm{M}}(t).$$

By the explicit representations obtained in Lemma 1, the minimum and maximum over one period can be written as

$$\min_{t\in[0,p]} \tilde{I}_{\mathrm{m}}(t) = \tilde{I}_{\mathrm{m}}(p) = D_2 W\left(\frac{\tilde{I}(0^+)}{D_2} \exp\left(\frac{\tilde{I}(0^+) - D_1 p}{D_2}\right)\right), \tag{3.18}$$

$$\max_{t\in[0,p]} \tilde{I}_{\mathrm{M}}(t) = \tilde{I}_M(0^+) = \frac{\varrho}{1 - M_1} + \frac{\sigma_1 k_0 D_2}{c_1 D_1 - \sigma_1 k_0},\ M_1 = \exp\left\{\frac{(D_1 - \sigma_1 \frac{k_0}{c_1})[\varrho - (D_1 - \sigma_1 \frac{k_0}{c_1})p]}{D_1 D_2}\right\}, \tag{3.19}$$

where we have used the same notations $\tilde{I}_{\mathrm{M}}(t)$ as in (3.9) and $\tilde{I}(t)$ as in (3.12).

In addition, for $t \neq kp$, the glucose equation can be written as

$$G'(t) = G_{\mathrm{in}} + b - \Big(\sigma_2 + aH(I(t))\Big)G(t).$$

Using

$$\tilde{I}_{\mathrm{m}}(p) \leq \liminf_{t\to\infty} I(t) \leq \limsup_{t\to\infty} I(t) \leq \tilde{I}_{\mathrm{M}}(0^+)$$

and the monotonicity of H, there exists $t^0 > 0$ such that for all $t \geq t^0$,

$$\kappa_{\min} \triangleq \sigma_2 + aH(\tilde{I}_{\mathrm{m}}(p)) \leq \sigma_2 + aH(I(t)) \leq \sigma_2 + aH(\tilde{I}_{\mathrm{M}}(0^+)) \triangleq \kappa_{\max}.$$

Hence,

$$(G_{\text{in}} + b) - \kappa_{\max} G(t) \le G'(t) = G_{\text{in}} + b - (\sigma_2 + aH(I(t)))G(t) \le (G_{\text{in}} + b) - \kappa_{\min} G(t),\ t \ge t^0.$$

Consider now the comparison equations

$$z_1'(t) = (G_{\text{in}} + b) - \kappa_{\max} z_1(t), \qquad z_1(t^0) = G(t^0),$$

$$z_2'(t) = (G_{\text{in}} + b) - \kappa_{\min} z_2(t), \qquad z_2(t^0) = G(t^0).$$

Their explicit solutions satisfy

$$\lim_{t\to\infty} z_1(t) = \frac{G_{\text{in}} + b}{\kappa_{\max}} \triangleq G_m, \qquad \lim_{t\to\infty} z_2(t) = \frac{G_{\text{in}} + b}{\kappa_{\min}} \triangleq G_M,$$

with $0 < G_m \le G_M$ since $\kappa_{\min} \le \kappa_{\max}$. By the comparison principle, we obtain

$$z_1(t) \le G(t) \le z_2(t), t \ge t^0,$$

and, hence,

$$G_m = \lim_{t\to\infty} z_1(t) \le \liminf_{t\to\infty} G(t) \le \limsup_{t\to\infty} G(t) \le \lim_{t\to\infty} z_2(t) = G_M.$$

Combining the bounds for $I(t)$ and $G(t)$ yields

$$G_m \le \liminf_{t\to\infty} G(t) \le \limsup_{t\to\infty} G(t) \le G_M, \qquad \tilde{I}_{\text{m}}(p) \le \liminf_{t\to\infty} I(t) \le \limsup_{t\to\infty} I(t) \le \tilde{I}_{\text{M}}(0^+).$$

Hence, all solutions with $(G_0, I_0) \in \mathbb{R}^2_+$ eventually enter and remain in the rectangle $[G_m, G_M] \times [\tilde{I}_{\text{m}}(p), \tilde{I}_{\text{M}}(0^+)] \subset \mathbb{R}^2_+$. This completes the proof.

Remark 2. *Theorem 2 shows that under the structural conditions, the long-term dynamics of system* (2.1) *are confined to the invariant rectangle* $\mathcal{R} = [G_m, G_M] \times [\tilde{I}_{\text{m}}(p), \tilde{I}_{\text{M}}(0^+)]$. *Specifically, bounds* G_m *and* G_M *depend on effective insulin action via* $\kappa_{\min} = \sigma_2 + aH(\tilde{I}_{\text{m}}(p))$, $\kappa_{\max} = \sigma_2 + aH(\tilde{I}_{\text{M}}(0^+))$, *while* $\tilde{I}_{\text{m}}(t)$ *and* $\tilde{I}_{\text{M}}(t)$ *are determined by injection period* p *and dose* ϱ. *Adjusting* p *and* ϱ *thus shifts and shrinks* $[G_m, G_M]$, *regulating the asymptotic blood glucose range. In particular, selecting* (p, ϱ) *such that* $[G_m, G_M] \subset [G^{\text{phys}}_{min}, G^{\text{phys}}_{max}]$ *for given physiological targets* $G^{\text{phys}}_{min}, G^{\text{phys}}_{max}$ *provides a model-based guideline to tune insulin therapy and maintain glucose within clinically acceptable levels.*

3.2. Dynamics of the state-dependent impulsive regulatory system

Having established the key dynamical properties of the periodically forced pump-therapy model (2.1), we proceed to the closed-loop case. In this subsection, we investigate the dynamical properties of system (2.2), with particular emphasis on the existence and stability of positive periodic orbits under the threshold-type state-feedback dosing rule.

Proposition 3. *Assume* $0 \le \sigma_1 \frac{k_0}{c_1} < D_1$, $(G_0, I_0) \in \mathbb{R}^2_+$, *and* $G_0 \le G_C$. *Then, system* (2.2) *admits a unique global solution* $(G(t), I(t))$ *for* $t \ge 0$, *which is positive and uniformly bounded.*

Proof. The global existence and uniqueness of solutions hold for system (2.2), by virtue of standard results on hybrid systems with locally Lipschitz continuous vector fields and continuous jump maps. The positivity argument is identical to that of Proposition 1, since the continuous dynamics of system (2.2) coincide with those of (2.1) and the jump map $(G, I) \mapsto (G, I + \varrho)$ preserves the nonnegative quadrant. Hence, $(G(t), I(t)) \in \mathbb{R}^2_+$ for all $t \geq 0$.

Similar to the discussion in Proposition 2, we obtain, for t between impulses,

$$G'(t) = G_{\text{in}} - \sigma_2 G(t) - aG(t)H(I(t)) + b \leq G_{\text{in}} + b - (\sigma_2 + ac)G(t).$$

As G does not jump at impulse times, the scalar comparison principle yields

$$0 \leq G(t) \leq \max\Big\{G_0, \frac{G_{\text{in}} + b}{\sigma_2 + ac}\Big\}, \qquad t \geq 0.$$

In addition, for t between impulses we have

$$I'(t) = F(G(t))\Phi(I(t)) - \frac{D_1 I(t)}{D_2 + I(t)} \leq \sigma_1 \frac{k_0}{c_1} - \frac{D_1 I(t)}{D_2 + I(t)} \triangleq \mathcal{F}(I(t)).$$

$\mathcal{F}$ has a unique positive zero $I^\Delta_M = \frac{\sigma_1 k_0 D_2}{c_1 D_1 - \sigma_1 k_0}$, and satisfies $\mathcal{F}(I) \leq 0$ for all $I \geq I^\Delta_M$.

Fix any interval $(t_k, t_{k+1}]$ between successive impulses, and consider the solution $\lambda(t)$ of

$$\lambda'(t) = \mathcal{F}(\lambda(t)), \qquad \lambda(t_k^+) = I(t_k^+).$$

By the scalar comparison principle, $I(t) \leq \lambda(t)$, $t \in (t_k, t_{k+1}]$. Since the equilibrium I^Δ_M of $\lambda'(t) = \mathcal{F}(\lambda)$ is globally attractive and the flow is monotone, it follows that $\lambda(t) \leq \max\{I(t_k^+), I^\Delta_M\}$, $t \in (t_k, t_{k+1}]$, and, hence,

$$I(t) \leq \max\{I(t_k^+), I^\Delta_M\}, \qquad t \in (t_k, t_{k+1}].$$

At each impulse time t_k, the jump rule of system (2.2) is

$$(G(t_k), I(t_k)) \in \Gamma = \{(G, I) : G = G_C,\ I \leq I_P\}, \quad I(t_k^+) = I(t_k) + \varrho,$$

so, in particular, $I(t_k^+) \leq I_P + \varrho$.

Combining this with the previous inequality yields

$$I(t) \leq \max\{I_0, I_P + \varrho, I^\Delta_M\}, \quad t \geq 0.$$

This completes the proof.

Before investigating the dynamics characteristics of system (2.2), we first analyze the underlying continuous-time system (with all impulses switched off)

$$\begin{cases} \dfrac{dG(t)}{dt} = G_{\text{in}} - \sigma_2 G(t) - aG(t)H(I(t)) + b = \bar{P}(G, I), \\ \dfrac{dI(t)}{dt} = F(G(t))\,\Phi(I(t)) - \Psi(I(t)) = \bar{Q}(G, I). \end{cases} \tag{3.20}$$

Lemma 2. *System* (3.20) *admits a unique positive equilibrium* $(\bar{G}, \bar{I})$*, which is globally asymptotically stable in* $\mathbb{R}^2_+$*. In particular, if* $\sigma_1 = 0$*, then* $(\bar{G}, \bar{I}) = (G^0, 0)$*,* $G^0 = \frac{G_{\text{in}} + b}{\sigma_2 + ac}$*.*

Proof. Obviously, if $\sigma_1 = 0$, then system (3.20) admits a unique equilibrium $(\bar{G}, \bar{I}) = (G^0, 0)$.

For $\sigma_1 > 0$, the equation $\bar{Q}(G, I) = 0$ can be written as

$$F(G)\,\Phi(I) = \Psi(I). \tag{3.21}$$

For fixed $G > 0$, the left-hand side of (3.21) is strictly decreasing in I (because Φ is positive and decreasing), while the righthand side is strictly increasing in I (because Ψ is positive and increasing). Moreover,

$$F(G)\Phi(0) = F(G)\frac{k_0}{c_1} > 0, \qquad \lim_{I\to\infty} F(G)\Phi(I) - \Psi(I) = -D_1 < 0.$$

Hence, for each $G > 0$ there exists a unique $I = \mathcal{I}(G) > 0$ satisfying (3.21).

Substituting $I = \mathcal{I}(G)$ into $\bar{P}(G, I) = 0$ gives a scalar equation in G

$$\tilde{\phi}(G) \triangleq G_{\text{in}} - \sigma_2 G - aG\,H(\mathcal{I}(G)) + b = 0.$$

By differentiating (3.21) with respect to G and using $F'(G) \geq 0$, $\Phi > 0$, $\Phi' < 0$, $\Psi' > 0$, one finds that $\mathcal{I}'(G) \geq 0$. Since H is increasing, this implies

$$\tilde{\phi}'(G) = -\sigma_2 - aH(\mathcal{I}(G)) - aGH'(\mathcal{I}(G))\,\mathcal{I}'(G) < 0, \qquad G \geq 0,$$

so $\tilde{\phi}$ is strictly decreasing on $(0, \infty)$. Furthermore,

$$\tilde{\phi}(0) = G_{\text{in}} + b > 0, \qquad \lim_{G\to\infty} \tilde{\phi}(G) = -\infty.$$

Therefore, by the intermediate value theorem there exists a unique $\bar{G} > 0$, solving $\tilde{\phi}(G) = 0$. Then, setting $\bar{I} = \mathcal{I}(\bar{G})$ yields a unique positive equilibrium $(\bar{G}, \bar{I})$ of (3.20).

A straightforward calculation gives the Jacobian matrix of (3.20) at $(\bar{G}, \bar{I})$ as

$$J(\bar{G}, \bar{I}) = \begin{pmatrix} -\sigma_2 - aH(\bar{I}) & -a\bar{G}\,H'(\bar{I}) \\ F'(\bar{G})\,\Phi(\bar{I}) & F(\bar{G})\,\Phi'(\bar{I}) - \Psi'(\bar{I}) \end{pmatrix}.$$

Here, $H(\bar{I}) > 0$, $H'(\bar{I}) > 0$, $F'(\bar{G}) \geq 0$, $\Phi(\bar{I}) > 0$, $\Phi'(\bar{I}) < 0$, and $\Psi'(\bar{I}) > 0$, so

$$\text{tr}\, J(\bar{G}, \bar{I}) = -\sigma_2 - aH(\bar{I}) + F(\bar{G})\,\Phi'(\bar{I}) - \Psi'(\bar{I}) < 0 \quad \text{and} \quad detJ(\bar{G}, \bar{I}) > 0.$$

By the Routh-Hurwitz criteria, $(\bar{G}, \bar{I})$ is locally asymptotically stable.

Moreover, we can easily get that all trajectories of (3.20) with $(G_0, I_0) \in \mathbb{R}^2_+$ remain bounded in $\mathbb{R}^2_+$. By choosing the Dulac function $B(G, I) \equiv 1$, we obtain, for all $(G, I) \in \mathbb{R}^2_+$,

$$\frac{\partial(B\bar{P})}{\partial G} + \frac{\partial(B\bar{Q})}{\partial I} = -(\sigma_2 + aH(I)) + [F(G)\,\Phi'(I) - \Psi'(I)] < 0.$$

The Bendixson-Dulac criterion then excludes nontrivial periodic orbits in $\mathbb{R}^2_+$. Then, the Poincaré-Bendixson theorem implies that every positive solution of (3.20) converges to $(\bar{G}, \bar{I})$ as $t \to \infty$. Thus, $(\bar{G}, \bar{I})$ is globally asymptotically stable in $\mathbb{R}^2_+$. This completes the proof.

The G-nullcline $P(G, I) = G'(t) = 0$ has a vertical asymptote $G = \frac{G_{\text{in}}+b}{\sigma_2+ac+am} \triangleq G_l$. In the subsequent analysis, we assume

$$G_l < G_C < \bar{G}$$

for the following reason. If $G_C \le G_l$, then the horizontal line $G = G_C$ does not intersect the G-nullcline and the threshold value I_P tends to $+\infty$. In system (2.2), this would imply that any trajectory starting below $G = G_C$ would experience infinitely many impulses and remain trapped on the line $G = G_C$, which is not physiologically meaningful. In addition, if $G_C \ge \bar{G}$, then no intervention is actually required: since the continuous system (3.20) tends to the equilibrium value $\bar{G}$, the glucose level would decrease below G_C without impulses.

Remark 3. *For the injection dose, we require*

$$I_P < \varrho.$$

Biologically, this condition means that a single bolus is large enough to drive the insulin level from the admissible injection region $\{I \le I_P\}$ into the inhibition region $\{I > I_P\}$. Thus, each hyperglycaemic excursion triggers at most one corrective bolus. This prevents insulin stacking at high plasma levels and matches the safety logic of artificial pancreas controllers.

To explore the periodic solutions for system (2.2), we first define a Poincaré map. Consider the vertical line

$$\Sigma \triangleq \{(G, I) : G = G_C,\ I \ge 0\},$$

and split it into two parts

$$\Sigma_{\text{imp}} \triangleq \{(G_C, I) : 0 \le I \le I_P\}, \qquad \Sigma_{\text{ph}} \triangleq \{(G_C, I) : I_P < I \le I_P + \varrho\},$$

which we call the impulse set and the phase set, respectively. We parametrize Σ_{ph} by the insulin coordinate $I \in (I_P, I_P + \varrho]$ and denote $Q = (G_C, I_Q)$ for points on this segment.

Since the vector field in (3.20) is locally Lipschitz and the jump rule $(G, I) \mapsto (G, I + \varrho)$ is continuous, system (2.2) is forward well posed. Moreover, using the same comparison arguments as in Proposition 3 (with periodic forcing removed), one can establish uniform positive bounds for $G(t)$ and $I(t)$ that hold for all $t \ge 0$, independent of the initial point $Q \in \Sigma_{\text{ph}}$. Hence, trajectories starting from Σ_{ph} remain in a fixed compact subset of $\mathbb{R}^2_+$.

Furthermore, since $(\bar{G}, \bar{I})$ is globally asymptotically stable for the underlying continuous system (3.20) (Lemma 2) and $G_l < G_C < \bar{G}$, any trajectory originating from a point $Q = (G_C, I_Q) \in \Sigma_{\text{ph}}$ first leaves Σ, enters the strip $G < G_C$, and then intersects the impulse segment Σ_{imp} at a unique time $t_1(Q) > 0$, with $(G(t_1^-), I(t_1^-)) \in \Sigma_{\text{imp}}$, and no impulse occurring on $(0, t_1)$. Denote this pre-impulse point by

$$Q_1' = (G_C, I_{Q_1'}) = (G(t_1^-), I(t_1^-)) \in \Sigma_{\text{imp}},$$

see Figure 1(a). The map

$$\mathcal{P}_1 : \Sigma_{\text{ph}} \to \Sigma_{\text{imp}}, \qquad \mathcal{P}_1(Q) = Q_1',$$

is therefore well defined and continuous.

At $t = t_1(Q)$, an impulse is applied and the state jumps satisfy

$$(G(t_1^+), I(t_1^+)) = (G_C, I_{Q_1'} + \varrho) = (G_C, I_{Q_1}) = Q_1 \in \Sigma_{\text{ph}},$$

because $0 \le I_{Q_1'} \le I_P$ and $I_P < \varrho$ imply $I_P < I_{Q_1'} + \varrho = I_{Q_1} \le I_P + \varrho$. Define the jump map

$$\mathcal{P}_2 : \Sigma_{\text{imp}} \to \Sigma_{\text{ph}}, \qquad \mathcal{P}_2(G_C, I) = (G_C, I + \varrho).$$

Then, the composition

$$\mathcal{P} \triangleq \mathcal{P}_2 \circ \mathcal{P}_1 : \Sigma_{\text{ph}} \to \Sigma_{\text{ph}}$$

is a well-defined continuous map, which we refer to as the Poincaré map. In terms of the insulin coordinate we write

$$\mathcal{P}(I_Q) = I_{Q_1'} + \varrho = I_{Q_1}, \qquad I_Q \in (I_P, I_P + \varrho].$$

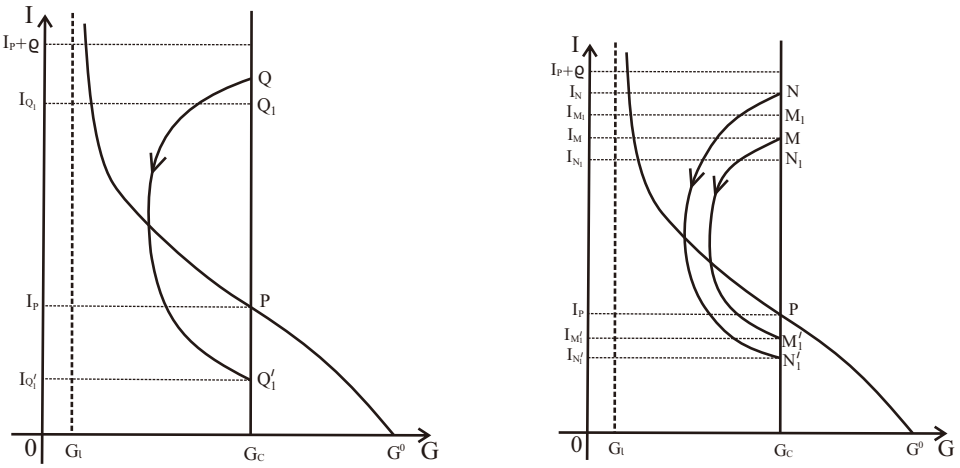

Figure 1. The existence and uniqueness of the order-1 periodic solution.

Clearly, the Poincaré map $\mathcal{P}$ maps the phase interval $(I_P, I_P + \varrho]$ into itself, and there is a one-to-one correspondence between its fixed points and the positive order-1 periodic solutions of system (2.2): each fixed point corresponds to exactly one positive order-1 periodic orbit (undergoing one impulse per period), and vice versa.

Theorem 3. *Suppose that $G_l < G_C < \bar{G}$ and $I_P < \varrho$. Then, system* (2.2) *admits a unique positive order-1 periodic solution.*

Proof. The qualitative behavior of trajectories of system (2.2) implies: for initial points $Q \in \Sigma_{\text{ph}}$ with I_Q close to the lower endpoint I_P, $\mathcal{P}(I_Q) > I_Q$; for I_Q close to the upper endpoint $I_P + \varrho$, $\mathcal{P}(I_Q) < I_Q$. More precisely, for any sufficiently small $\varepsilon > 0$, we can select $I^- \in (I_P, I_P + \varepsilon)$ and $I^+ \in (I_P + \varrho - \varepsilon, I_P + \varrho)$ such that

$$\mathcal{P}(I^-) > I^-, \qquad \mathcal{P}(I^+) < I^+.$$

Since $\mathcal{P}$ is continuous on $(I_P, I_P + \varrho]$, there must exist a point $I_T \in (I_P, I_P + \varrho)$ such that

$$\mathcal{P}(I_T) = I_T.$$

Let $T = (G_C, I_T) \in \Sigma_{\text{ph}}$ denote the corresponding point on the phase set. By construction, the trajectory originating from T is a positive order-1 periodic orbit of system (2.2).

To prove uniqueness, we show that $\mathcal{P}$ is strictly monotone on $(I_P, I_P+\varrho]$. Consider two initial points $M = (G_C, I_M)$ and $N = (G_C, I_N)$ in Σ_{ph} with $I_M < I_N$. As illustrated in Figure 1(b), the corresponding trajectories of (2.2) cannot intersect and the orbit starting from N returns to the impulse segment Σ_{imp} at a lower insulin level than the orbit starting from M. In particular, if we denote the corresponding pre-impulse points by $M_1' = (G_C, I_{M_1'}), N_1' = (G_C, I_{N_1'}) \in \Sigma_{\text{imp}}$, then $I_{M_1'} > I_{N_1'}$. Therefore,

$$\mathcal{P}(I_M) = I_{M_1'} + \varrho > I_{N_1'} + \varrho = \mathcal{P}(I_N),$$

so $\mathcal{P}$ is strictly decreasing on $(I_P, I_P + \varrho]$. A strictly monotone continuous map on an interval has at most one fixed point. Since the existence of at least one fixed point I_T has already been established above, this fixed point is unique. Consequently, the state-dependent impulsive system (2.2) admits a unique positive order-1 periodic orbit, which corresponds to the unique fixed point of the Poincaré map $\mathcal{P}$. This completes the proof.

Let $T = (G_C, I_T) \in \Sigma_{\text{ph}}$ be the intersection point of the unique positive order-1 periodic orbit $\widetilde{\Gamma}$ with the phase section $\Sigma_{\text{ph}} = (I_P, I_P + \varrho]$, and let $Q_0 = (G_C, I_{Q_0})$ with $I_{Q_0} = I_P + \varrho$ denote the upper endpoint of Σ_{ph}. Then, we have the following result.

Theorem 4. *Assume that $G_l < G_C < \bar{G}$ and $I_P < \varrho$. Then, the unique order-1 periodic orbit $\widetilde{\Gamma}$ of system* (2.2) *is globally orbitally asymptotically stable in the strip*

$$\mathcal{S} \triangleq \{(G, I) \in \mathbb{R}^2_+ :\ 0 \le G \le G_C,\ I \ge 0\}.$$

Proof. We first prove that the trajectory of system (2.2) starting from Q_0 converges to the order-1 periodic orbit $\widetilde{\Gamma}$. To this end, define the iterates on the phase section

$$Q_{k+1} = \mathcal{P}(Q_k) = \mathcal{P}(G_C, I_{Q_k}) = \mathcal{P}^{k+1}(Q_0), \quad k = 0, 1, 2, \ldots.$$

Since $I_P < I_T < I_Q$, strict monotonicity of $\mathcal{P}$ and the phase portrait geometry in Figure 2 imply that the successive intersection points $\{Q_k\}$ alternate on Σ_{ph} around T: the odd-indexed points lie between I_P and I_T, while the even-indexed points lie between I_T and I_{Q_0}. More precisely, one obtains the two interlaced chains of inequalities

$$I_P < I_{Q_1} < I_{Q_3} < \cdots < I_{Q_{2k-1}} < \cdots < I_T < \cdots < I_{Q_{2k}} < \cdots < I_{Q_2} < I_{Q_0}. \tag{3.22}$$

The odd subsequence $\{I_{Q_{2k-1}}\}_{k\ge1}$ is strictly increasing and bounded above by I_T, whereas the even subsequence $\{I_{Q_{2k}}\}_{k\ge1}$ is strictly decreasing and bounded below by I_T. Thus,

$$\lim_{k\to\infty} I_{Q_{2k-1}} = \lim_{k\to\infty} \mathcal{P}(I_{Q_{2k}}) = I_T. \tag{3.23}$$

Therefore, $\lim_{k\to\infty} I_{Q_k} = I_T$.

Since the sequence $\{I_{Q_k}\}$ records the successive intersections of the trajectory from Q_0 with the phase section Σ_{ph}, its convergence to I_T implies that this trajectory converges to the unique order-1 periodic orbit $\widetilde{\Gamma}$.

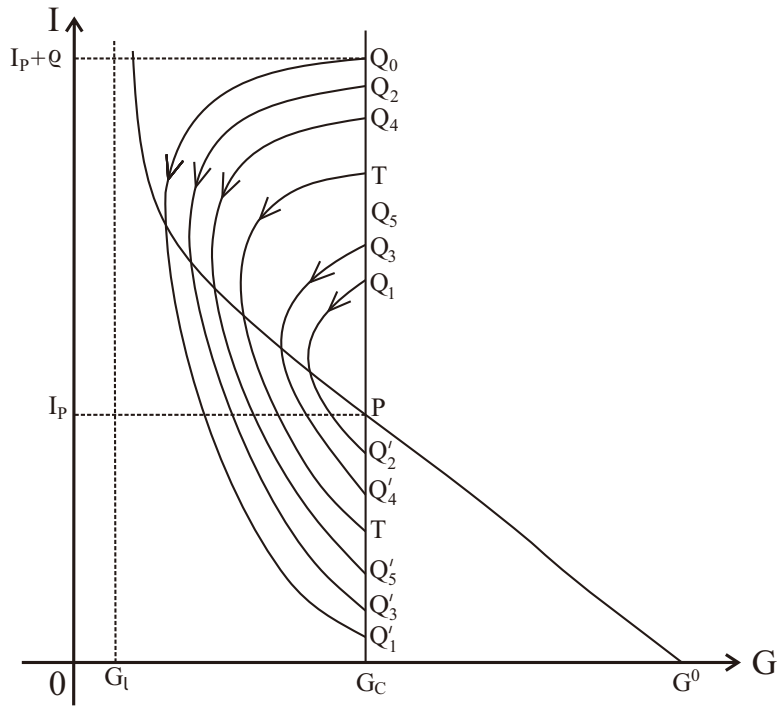

Figure 2. The attractivity of the positive order-1 periodic orbit.

Let $V_0 = (G_C, I_{V_0}) \in \Sigma_{\text{ph}}$ be arbitrary. If $I_{V_0} = I_T$, then $V_\ell \equiv T(\ell = 0, 1, 2, \cdots)$, so we assume $I_{V_0} \neq I_T$. If $I_P < I_{V_0} < I_{Q_1}$, the strict monotonic decrease of $\mathcal{P}$ and its invariance on $(I_P, I_{Q_0}]$ yield

$$I_{Q_1} = \mathcal{P}(I_{Q_0}) \leq \mathcal{P}(I_{V_0}) = I_{V_1} \leq \mathcal{P}(I_P) \leq I_{Q_0},$$

that is, $I_{V_1} \in [I_{Q_1}, I_{Q_0}]$. Thus, the trajectory from V_0 intersects the segment $\overline{Q_1 Q_0} \subset \Sigma_{\text{ph}}$ after one impulse, so we only need to consider the case $I_{Q_1} \leq I_{V_0} \leq I_{Q_0}$ without loss of generality. We first treat

$$I_{Q_1} \leq I_{V_0} < I_T. \tag{3.24}$$

From the strict ordering of the odd subsequence

$$iI_{Q_1} < I_{Q_3} < \cdots < I_{Q_{2k-1}} < \cdots < I_T,$$

and the inequality (3.24), there exists an integer $i_0 \geq 1$ such that

$$I_{Q_{2i_0-1}} \leq I_{V_0} < I_{Q_{2i_0+1}} < I_T. \tag{3.25}$$

Geometrically, V_0 lies on the segment between Q_{2i_0-1} and Q_{2i_0+1} on the phase section.

Define the iterates $V_{\ell+1} = \mathcal{P}(V_\ell)$ and denote by I_{V_ℓ} the insulin coordinate of V_ℓ, $\ell = 0, 1, 2, \ldots$. We can easily obtain that for all $l \geq 0$,

$$I_{Q_{2(i_0+\ell)-1}} \leq I_{V_{2\ell}} < I_{Q_{2(i_0+\ell)+1}}, \quad I_{Q_{2(i_0+\ell)}} \geq I_{V_{2\ell+1}} > I_{Q_{2(i_0+\ell)+2}}. \tag{3.26}$$

According to (3.23), we know that

$$\lim_{\ell\to\infty} I_{Q_{2(i_0+\ell)-1}} = \lim_{\ell\to\infty} I_{Q_{2(i_0+\ell)+1}} = I_T, \quad \lim_{\ell\to\infty} I_{Q_{2(i_0+\ell)}} = \lim_{\ell\to\infty} I_{Q_{2(i_0+\ell)+2}} = I_T.$$

Hence, by the squeezing relations (3.26),

$$\lim_{\ell\to\infty} I_{V_{2\ell}} = \lim_{\ell\to\infty} I_{V_{2\ell+1}} = I_T,$$

and, therefore, the full sequence $\{I_{V_\ell}\}_{\ell\geq 0}$ converges to I_T.

The case $I_T < I_{V_0} \leq I_{Q_0}$ can be treated in the same way, by initially placing V_0 between two consecutive even points Q_{2i_0} and Q_{2i_0+2} and interchanging the roles of the odd and even subsequences. The same squeezing argument shows that $I_{V_\ell} \to I_T$ as $\ell \to \infty$.

Consequently, for any starting point $V_0 \in \Sigma_{\text{ph}}$, the successive intersection points V_ℓ of the corresponding trajectory of system (2.2) with the phase section converge to $T = (G_C, I_T)$. This means that the trajectory approaches the unique positive order-1 periodic orbit $\widetilde{\Gamma}$.

Finally, analogous to the discussion in Proposition 3, any solution starting from $\mathcal{S}$ remains in it. Using the phase portrait of the continuous subsystem (3.20) and the structure of the impulse set, the assumptions $G_l < G_C < \bar{G}$ and $I_P < \varrho$ imply that any trajectory originating from a point in $\mathcal{S} \setminus \Sigma_{\text{ph}}$ reaches the phase set Σ_{ph} after a finite time and finitely many impulses. Once the trajectory enters Σ_{ph}, the above analysis shows that it converges, up to a phase shift, to the order-1 periodic orbit $\widetilde{\Gamma}$.

Therefore, every solution of system (2.2) with $(G_0, I_0) \in \mathcal{S}$ converges orbitally to $\widetilde{\Gamma}$ as $t \to \infty$. Thus, $\widetilde{\Gamma}$ is globally orbitally asymptotically stable in $\mathcal{S}$. This completes the proof.

Remark 4. *Theorem 4 establishes that the order-1 periodic orbit $\widetilde{\Gamma}$ is globally orbitally asymptotically stable in the strip $\mathcal{S} = \{(G, I) \in \mathbb{R}^2_+ : 0 \leq G \leq G_C,\ I \geq 0\}$. This means that $\mathcal{S}$ is precisely the domain of attraction. From a physiological perspective, the strip $\mathcal{S}$ represents a clinically relevant operating region for the artificial pancreas, where glucose levels stay below the threshold G_C. Theorem 4 demonstrates that under the design criteria $G_l < G_C < \bar{G}$ and $I_P < \varrho$, the closed-loop system has a unique order-1 periodic orbit $\widetilde{\Gamma}$ that attracts all trajectories in $\mathcal{S}$. Notably, proper selection of the glucose threshold G_C and bolus dose ϱ ensures that all admissible initial states in $\mathcal{S}$ converge to a stable, repetitive glucose-insulin dynamic pattern, enabling long-term effective and self-regulating insulin therapy.*

4. Numerical simulations

This section presents numerical simulations to illustrate the dynamical properties of the two impulsive regulatory systems and to complement the theoretical results. Unless otherwise specified, all parameter values follow Table 2, which are taken from or adapted to be consistent with previous glucose-insulin modeling studies [8, 12, 21], with minor unit conversions. The IDE-related parameters (k_0, c_1) and the clearance parameters (D_1, D_2) are chosen such that the steady-state glucose and insulin levels fall in realistic physiological ranges for hyperglycaemic patients.

The numerical simulations in this section serve three purposes: (i) to visually confirm the theoretical results established in Section 3 (Theorems 1–4); (ii) to illustrate how key parameters $(p, \varrho, G_C, k_0, D_1)$ influence the long-term glycemic dynamics; and (iii) to provide clinically interpretable insights, such as the identification of safe dosing regions and the comparison of different delivery strategies.

Table 2. Model parameter values.

Parameter	Value	Unit	Parameter	Value	Unit
G_{in}	216	mg/min	b	100	mg
σ_1	6.27	mU/min	σ_2	5×10^{-6}	min^{-1}
a	4×10^{-5}	mg^{-1}	c	40	mg/min
m	900	mg/min	n	80	mg
α_1	105	mg	c_1	0.06	-
k_0	0.10	min^{-1}	D_1	150	min^{-1}
D_2	2300	min^{-1}	-	-	-

Based on this baseline parameter set, we first examine the long-term behavior of the periodic pump-therapy model (2.1). For T1DM, we fix $\sigma_1 = 0$, and we set the dosing period to $p = 30$ min and the bolus size to $\varrho = 0.5$ U, which satisfies the condition $\varrho < D_1 p$ in Theorem 1. Figure 3 depicts the corresponding solution trajectories of system (2.1) starting from four distinct initial states. This figure illustrates the global asymptotic stability of the unique positive periodic solution for T1DM as proved in Theorem 1. Trajectories from four distinct initial conditions converge to the same p-periodic solution $(\tilde{G}(t), \tilde{I}(t))$.

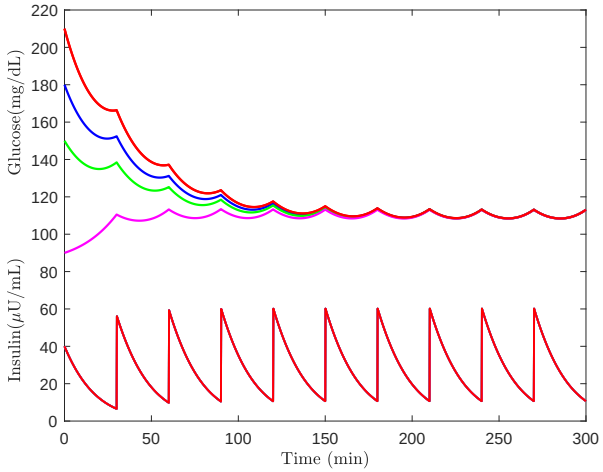

Figure 3. The global asymptotic stability of the positive periodic solution of system (2.1) for T1DM.

Figure 4 illustrates the dosing-parameter constraints from Theorem 2 for T2DM with $\sigma_1 = 6.27$. For each admissible pair (p, ϱ) satisfying $\varrho < (D_1 - \sigma_1 k_0/c_1)p$, we calculate the bounds $G_m(p, \varrho)$ and $G_M(p, \varrho)$, which denote the long-term glucose oscillation limits of system (2.1). We adopt the physiologically acceptable thresholds $G_{\text{min}}^{\text{phys}} = 85$ mg/dL and $G_{\text{max}}^{\text{phys}} = 150$ mg/dL. The shaded area between the curves $G_m(p, \varrho) = 85$ and $G_M(p, \varrho) = 150$ is exactly the dosing schedule set where the permanence rectangle of Theorem 2 meets

$$G_m(p, \varrho) \geq 85 \text{ mg/dL}, \qquad G_M(p, \varrho) \leq 150 \text{ mg/dL}.$$

In this region, the impulse period p and bolus size ϱ together prevent chronic hyperglycaemia and

treatment-induced hypoglycaemia over the long term.

The safe dosing region in Figure 4 has direct clinical relevance: any combination of dosing period p and bolus size ϱ lying inside this region guarantees that the patient's long-term glucose levels remain within the target range [85, 150] mg/dL. This provides a quantitative guideline for clinicians to adjust pump settings based on individual patient characteristics.

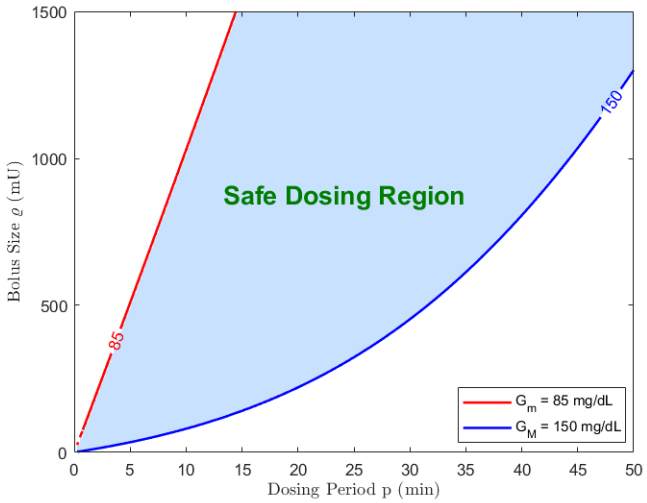

Figure 4. The safe dosing region in the (p, ϱ)-plane for T2DM with periodic pump-therapy.

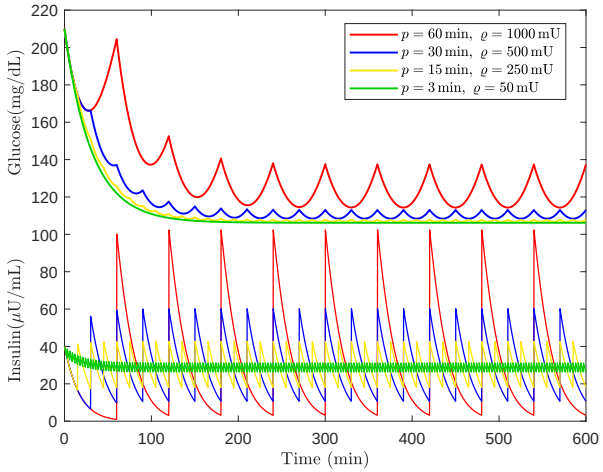

Figure 5. The insulin dosing strategies under a fixed total insulin amount for periodic pump-therapy.

To compare insulin dosing strategies under a fixed total insulin amount, we systematically vary the dosing period p and bolus size ϱ while maintaining a constant mean infusion rate ϱ/p. Figure 5 illustrates four representative regimens, all starting from identical initial values. Although the total insulin delivered per unit time remains the same across all four cases, the different temporal distribution yields markedly distinct long-term glycaemic patterns.

When insulin is administered as infrequent, large boluses ($p = 60$ min, $\varrho = 1000$ mU), the model predicts pronounced glucose oscillations accompanied by relatively high pre-injection peaks and a comparatively elevated average glucose level. As the dosing frequency increases and the bolus size decreases, both the amplitude and the mean level of glucose are progressively reduced. In the extreme case of very frequent, small boluses ($p = 3$ min, $\varrho = 50$ mU), the glucose trajectory settles into a lower, nearly flat periodic orbit. Hence, even with an identical total insulin input, small high-frequency boluses afford superior hyperglycaemia control by lowering the overall steady-state glycaemic level and suppressing large glucose excursions. This finding aligns with clinical preferences for smooth pump-based delivery over high-dose intermittent injections in diabetes management.

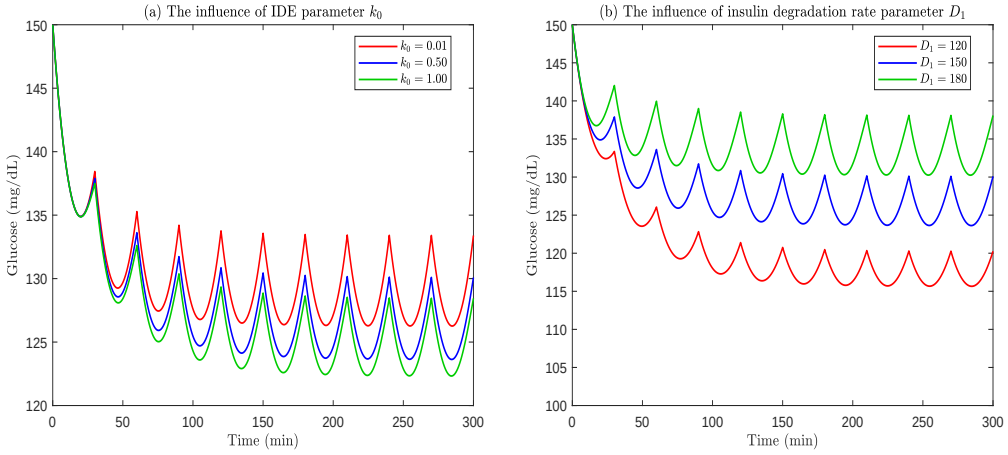

Figure 6. Sensitivity analysis of IDE-related parameters. (a) Influence of k_0 on glucose dynamics; (b) Influence of D_1 on glucose dynamics.

We further examined how two key parameters affect glycemic dynamics: k_0 (IDE modulation scale) and D_1 (maximum insulin degradation rate). Simulations used the periodic pump model for type II diabetes with fixed dosing ($p = 30$ min, $\varrho = 500$ mU). Figure 6(a) shows that increasing k_0 (from 0.01 to 1.00) elevates glucose levels and widens excursions, because stronger IDE modulation reduces effective insulin availability. Thus, patients with high IDE activity may need larger or more frequent doses. In panel (b), raising D_1 (from 120 to 180 min^{-1}) also raises glucose, as faster insulin clearance shortens its action. Conversely, lower D_1 prolongs insulin effect and improves control. These trends match physiological expectations and confirm that individualized therapy should account for IDE activity and degradation capacity. Importantly, the stability and permanence results (Theorems 1 and 2) remain valid across the tested parameter ranges, underscoring their robustness.

In the second set of simulations, we focus on the state-dependent impulsive model (2.2). We fix the glucose threshold at $G_C = 150$ mg/dL and select the impulse dose ϱ to satisfy the hypotheses of Theorems 3 and 4, namely, $G_l < G_C < \bar{G}$ and $I_P < \varrho$.

From Figure 7, we see that trajectories starting from disparate glucose and insulin levels evolve continuously below G_C, hit $G = G_C$ at different times to trigger impulses with distinct transients, and then converge to the same periodic regime after several impulses. This confirms the unique order-1 periodic solution is globally orbitally asymptotically stable. From a physiological perspective, this also demonstrates the robustness of threshold-based closed-loop insulin therapy. When control parameters

(G_C, ϱ) are set to satisfy Theorems 3 and 4, the artificial pancreas system automatically steers glucose-insulin dynamics toward a stable periodic pattern. Glucose is confined to a narrow range below the safety threshold G_C, even with widely varying initial glucose and insulin levels.

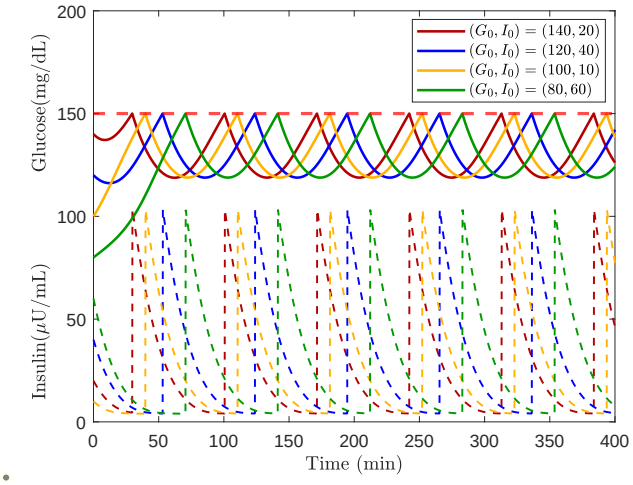

Figure 7. The global orbital stability of the order-1 periodic solution of system (2.2).

Figure 8 shows two distinct order-1 periodic orbits of the state-dependent impulsive system (2.2), both corresponding to the same glucose threshold $G_C = 150$ mg/dL but different bolus sizes: $\varrho = 300$ mU and $\varrho = 600$ mU. In each case, the solution converges to a unique periodic orbit. The resulting glucose profiles, however, differ markedly. The trajectory for the larger bolus ($\varrho = 600$ mU) lies consistently below that for the smaller one ($\varrho = 300$ mU) over most of the cycle. This demonstrates that, for a fixed feedback threshold G_C, a larger corrective bolus produces a stronger reduction of hyperglycaemia and maintains blood glucose within a lower range for a longer duration. Clinically, this implies that increasing the bolus size in a threshold-based closed-loop therapy can substantially improve hyperglycaemia control compared to smaller, more conservative corrections.

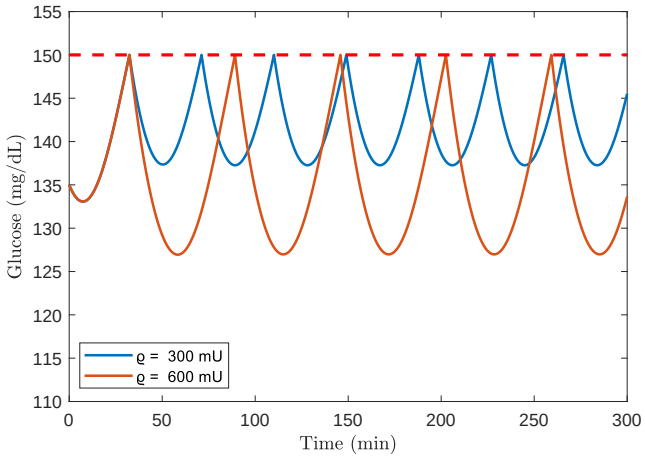

Figure 8. Comparison of order-1 periodic orbits of system (2.2) with different bolus size ϱ.

5. Conclusions

In this work we proposed and analyzed two glucose-insulin models describing impulsive treatment by exogenous insulin. The first model represents periodic bolus delivery via an insulin pump, while the second model captures state-dependent dosing in a closed-loop artificial pancreas. Both models incorporate a Michaelis-Menten type degradation of insulin and an IDE-modulated production term, so that they remain physiologically interpretable yet flexible enough to describe insulin therapy.

For the periodic pump model, we established global well-posedness, positivity, and boundedness of solutions. In the type I diabetes case ($\sigma_1 = 0$) we proved the existence of a unique positive p-periodic solution which is globally asymptotically stable. For the type II case ($\sigma_1 > 0$) we derived explicit positive lower and upper bounds for both glucose and insulin, and obtained a permanence result which allows us to delineate a safe dosing region in the (p, ϱ)-plane. For the state-dependent impulsive model, under mild structural conditions on the glucose threshold and safety level, we proved that the full hybrid system admits a unique positive order-1 periodic orbit, and that this orbit is globally orbitally asymptotically stable in a biologically relevant strip. Thus, any trajectory starting below the threshold ultimately converges to a regular pattern of threshold-triggered pulses.

The impulsive effects in both models play a dual role: they provide the necessary exogenous insulin to compensate for deficient endogenous secretion, and they act as a stabilizing force that drives the system toward a predictable, bounded, and clinically acceptable dynamic regime. In the periodic model, the impulses create a globally attractive periodic solution; in the state-dependent model, they enforce a glucose ceiling and yield a globally stable order-1 periodic orbit. These findings mathematically formalize the intuitive notion that properly timed and dosed insulin injections can stabilize glycemic dynamics in diabetic patients.

The stability and permanence results have direct clinical implications. For type I diabetes, the global asymptotic stability of the periodic solution guarantees that, under fixed pump settings, the glucose-insulin dynamics will converge to a predictable pattern, enabling reliable long-term control. For type II diabetes, the permanence bounds define a safe dosing region where glucose remains within physiological limits, thus preventing both hyperglycemia and hypoglycemia. In the state-dependent model, the global orbital stability of the order-1 periodic orbit ensures that the artificial pancreas system, once triggered by a glucose threshold, will automatically steer the patient toward a stable glycemic pattern, regardless of initial conditions. These findings support the use of model-based tuning of insulin pump and artificial pancreas parameters to achieve personalized therapy.

Numerical simulations were performed to illustrate and complement the theoretical results. These simulations confirm the global attraction of the periodic solution in the pump model and visualize the safe dosing region predicted by the permanence theorem. They also demonstrate how varying the dosing period and bolus size splits the same total dose into qualitatively distinct glycemic profiles. For the state-dependent model, simulations demonstrate the global orbital stability of the order-1 periodic orbit, and highlight that larger corrective boluses can maintain lower glucose levels for a longer duration per cycle. Altogether, the analysis suggests that mathematically guided tuning of dosing period, bolus size, and threshold values can offer useful insight for designing personalized insulin pump and artificial pancreas strategies for glycaemia control.

Use of AI tools declaration

The authors declare they have not used Artificial Intelligence (AI) tools in the creation of this article.

Acknowledgments

This work is supported by the National Natural Science Foundation of China (12271466), Natural Science Foundation of Henan Province (252300420346) and Scientific Research Foundation of Graduate School of Xinyan Normal University (2025KYJJ57).

Conflict of interest

The authors declare there are no conflicts of interest.

References

1. C. Chen, H. Tsai, Modeling the physiological glucose-insulin system on normal and diabetic subjects, *Comput. Methods Programs Biomed.*, **97** (2010), 130–140. https://doi.org/10.1016/j.cmpb.2009.06.005
2. A. Boutayeb, A. Chetouani, A critical review of mathematical models and data used in diabetology, *Biomed. Eng. Online*, **5** (2006), 43. https://doi.org/10.1186/1475-925X-5-43
3. P. Palumbo, S. Ditlevsen, A. Bertuzzi, A. Gaetano, Mathematical modeling of the glucose-insulin system: A review, *Math. Biosci.*, **244** (2013), 69–81. https://doi.org/10.1016/j.mbs.2013.05.006
4. F. A. Rihan, *Delay Differential Equations and Applications to Biology*, 1st edition, Springer, 2021. https://doi.org/10.1007/978-981-16-0626-7
5. F. A. Rihan, K. Udhayakumar, Optimal control of glucose-insulin dynamics via delay differential model with fractional-order, *Alexandria Eng. J.*, **114** (2025), 243–255. https://doi.org/10.1016/j.aej.2024.11.071
6. S. Liu, G. Lv, Almost sure polynomial stability and stabilization of stochastic differential systems with impulsive effects, *Stat. Probab. Lett.*, **206** (2024), 109980. https://doi.org/10.1016/j.spl.2023.109980
7. F. A. Rihan, K. Udhayakumar, S. F. Nasrin, C. Rajivganthi, A stochastic delay differential model for glucose-insulin interactions, *Ain Shams Eng. J.*, **16** (2025), 103668. https://doi.org/10.1016/j.asej.2025.103668
8. M. Z. Huang, J. X. Li, X. Y. Song, H. J. Guo, Modeling impulsive injections of insulin: Towards artificial pancreas, *SIAM J. Appl. Math.*, **72** (2012), 1524–1548. https://doi.org/10.1137/110860306
9. X. Y. Song, M. Z. Huang, J. X. Li, Modeling impulsive insulin delivery in insulin pump with time delays, *SIAM J. Appl. Math.*, **74** (2014), 1763–1785. https://doi.org/10.1137/130933137
10. C. T. Li, Y. T. Liu, X. Z. Feng, Y. Z. Wang, Dynamic analysis of a class of insulin-glucose-glucocorticoid model with nonlinear pulse, *Nonlinear Anal. Real World Appl.*, **85** (2025), 104352. https://doi.org/10.1016/j.nonrwa.2025.104352

11. M. Koschorreck, E. D. Gilles, Mathematical modeling and analysis of insulin clearance in vivo, *BMC Syst. Biol.*, **2** (2008), 43. https://doi.org/10.1186/1752-0509-2-43

12. H. Y. Wang, J. X. Li, Y. Kuang, Enhanced modelling of the glucose-insulin system and its applications in insulin therapies, *J. Biol. Dyn.*, **3** (2009), 22–38. https://doi.org/10.1080/17513750802101927

13. C. T. Li, Y. T. Liu, Y. Z. Wang, X. Z. Feng, Dynamic modeling of the glucose-insulin system with inhibitors impulsive control, *Math. Methods Appl. Sci.*, **2024** (2024), 20907267. https://doi.org/10.1002/mma.10266

14. S. Y. Tang, Y. N. Xiao, One-compartment model with Michaelis-Menten elimination kinetics and therapeutic window: An analytical approach, *J. Pharmacokinet. Pharmacodyn.*, **34** (2007), 807–827. https://doi.org/10.1007/s10928-007-9070-4

15. S. M. Alzahrani, Statistical insights into stochastic glucose-insulin dynamics: Modeling insulin degradation with the Michaelis-Menten function, *Eur. J. Pure Appl. Math.*, **18** (2025), 5404. https://doi.org/10.29020/nybg.ejpam.v18i1.5404

16. W. Farris, S. Mansourian, Y. Chang, L. Lindsley, E. A. Eckman, M. P. Frosch, et al., Insulin-degrading enzyme regulates the levels of insulin, amyloid β-protein, and the β-amyloid precursor protein intracellular domain in vivo, *Proc. Natl. Acad. Sci. U.S.A.*, **100** (2003), 4162–4167. https://doi.org/10.1073/pnas.0230450100

17. O. Pivovarova, A. H*ö*hn, T Grune, A. Pfeiffer, N. Rudovich, Insulin-degrading enzyme: New therapeutic target for diabetes and Alzheimer's disease?, *Ann. Med.*, **48** (2016), 614–624. https://doi.org/10.1080/07853890.2016.1197416

18. M. A. Leissring, C. M. González-Casimiro, B. Merino, C. N. Suire, G. Perdomo, Targeting insulin-degrading enzyme in insulin clearance, *Int. J. Mol. Sci.*, **22** (2021), 2235. https://doi.org/10.3390/ijms22052235

19. G. Tundo, D. Sbardella, C. Ciaccio, G. Grasso, M. Gioia, A. Coletta, et al., Multiple functions of insulin-degrading enzyme: A metabolic crosslight?, *Crit. Rev. Biochem. Mol. Biol.*, **52** (2017), 554–582. https://doi.org/10.1080/10409238.2017.1337707

20. A. Mari, A. Tura, E. Grespan, R. Bizzotto, Mathematical modeling for the physiological and clinical investigation of glucose homeostasis and diabetes, *Front. Physiol.*, **11** (2020), 575789. https://doi.org/10.3389/fphys.2020.575789

21. F. Rao, Z. L. Zhang, J. X. Li, Dynamical analysis of a glucose-insulin regulatory system with insulin-degrading enzyme and multiple delays, *J. Math. Biol.*, **87** (2023), 73. https://doi.org/10.1007/s00285-023-02003-6

22. C. M. González-Casimiro, B. Merino, E. Casanueva-Álvarez, T. Postigo-Casado, P. Cámara-Torres, C. M. Fernández-Daz, et al., Modulation of insulin sensitivity by insulin-degrading enzyme, *Biomedicines*, **9** (2021), 86. https://doi.org/10.3390/biomedicines9010086

23. J. Yang, S. Y. Tang, R. A. Cheke, The regulatory system for diabetes mellitus: Modeling rates of glucose infusions and insulin injections, *Commun. Nonlinear Sci. Numer. Simul.*, **37** (2016), 305–325. https://doi.org/10.1016/j.cnsns.2016.02.001

24. J. Yang, S. Y. Tang, R. A. Cheke, Modelling the regulatory system for diabetes mellitus with a threshold window, *Commun. Nonlinear Sci. Numer. Simul.*, **22** (2015), 478–491. https://doi.org/10.1016/j.cnsns.2014.08.012

25. C. T. Li, J. Tian, X. Z. Feng, Y. T. Liu, Study on dynamical behavior of a type of diabetes mellitus model with nonlinear impulsive injection of insulin, *Math. Methods Appl. Sci.*, **48** (2025), 16765–16777. https://doi.org/10.1002/mma.70125

26. J. Jia, Z. Zhao, J. G. Yang, A. Zeb, Parameter estimation and global sensitivity analysis of a bacterial-plasmid model with impulsive drug treatment, *Chaos, Solitons Fractals*, **183** (2024), 114901. https://doi.org/10.1016/j.chaos.2024.114901

27. Q. Li, B. W. Liu, Traveling wave fronts to a Mackey-Glass model involving distinct delays in diffusion term and birth function, *Math. Methods Appl. Sci.*, **48** (2025), 15549–15558. https://doi.org/10.1002/mma.11109

28. D. D. Bainov, P. S. Simeonov, *System with Impulse Effect: Stability, Theory and Applications*, Ellis Horwood, Chichester, 1989.

29. X. D. Li, M. Bohner, C. K. Wang, Impulsive differential equations: periodic solutions and applications, *Automatica*, **52** (2015), 173–178. https://doi.org/10.1016/j.automatica.2014.11.009

30. G. Yang, L. G. Yao, Positive almost periodic solutions for an epidemic model with saturated treatment, *Taiwanese J. Math.*, **20** (2016), 1377–1392. https://doi.org/10.11650/tjm.20.2016.7639

31. G. Yang, Dynamical behaviors on a delay differential neoclassical growth model with patch structure, *Math. Methods Appl. Sci.*, **41** (2018), 3856–3867. https://doi.org/10.1002/mma.4872

Appendix

A.1. The proof of Lemma 1

Proof. (i) Assume $a_1 \geq b_1$. Since $\dfrac{u}{c_2+u} \leq 1$ for $u \geq 0$, we have

$$u'(t) = a_1 - \frac{b_1 u(t)}{c_2 + u(t)} \geq a_1 - b_1 \geq 0, \qquad t \neq kp.$$

Thus, $u(t)$ is nondecreasing along each continuous segment. At every impulse time, $u(t_k^+) = u(t_k) + \varrho \geq u(t_k)$, so the overall solution is nondecreasing in t. Moreover, since $\varrho > 0$ implies $u((k+1)p^+) \geq u(kp^+) + \varrho$, it follows that $u(kp^+) \to +\infty$ as $k \to \infty$, hence $u(t)$ is unbounded.

(ii) Assume $0 \leq a_1 < b_1$, $\varrho < (b_1 - a_1)p$ and denote $r \triangleq b_1 - a_1 > 0$. Fix an integer k, and consider the flow of model (3.1) on $(kp^+, (k+1)p]$ with initial value $u(kp^+) = u_k > 0$. For $t \in (kp^+, (k+1)p]$, the differential equation can be rewritten as

$$\frac{du}{dt} = \frac{a_1 c_2 - ru}{c_2 + u}. \tag{A1}$$

Separating variables yields

$$dt = \frac{c_2 + u}{a_1 c_2 - ru}\, du = \left(-\frac{1}{r} + \frac{b_1 c_2}{r} \cdot \frac{1}{a_1 c_2 - ru} \right) du. \tag{A2}$$

From (A1), we know that for all $t \in (kp^+, (k+1)p]$, if $u_k > (=, <)\frac{a_1c_2}{r}$, then $u(t) > (=, <)\frac{a_1c_2}{r}$ holds. That is to say, $\operatorname{sgn}(a_1c_2 - ru(t)) = \operatorname{sgn}(a_1c_2 - ru_k)$ for $t \in (kp^+, (k+1)p)$. Take the case where $u_k < \frac{a_1c_2}{r}$ as an example (the case where $u_k > \frac{a_1c_2}{r}$ can be derived analogously), and integrate both sides of (A2) from kp to t, yielding

$$u(t) + \frac{b_1c_2}{r}\ln\left(a_1c_2 - ru(t)\right) = u_k + \frac{b_1c_2}{r}\ln\left(a_1c_2 - ru_k\right) - r(t - kp). \tag{A3}$$

By standard algebraic manipulations, (A3) can be equivalently transformed into

$$-\frac{r}{b_1c_2}\left(\frac{a_1c_2}{r} - u(t)\right) + \ln\left(\frac{a_1c_2}{r} - u(t)\right) = -\frac{r}{b_1c_2}\left(\frac{a_1c_2}{r} - u_k\right) + \ln\left(\frac{a_1c_2}{r} - u_k\right) - \frac{r^2}{b_1c_2}(t - kp),$$

then we can deduce

$$\exp\left(-\frac{r}{b_1c_2}\left(\frac{a_1c_2}{r} - u(t)\right)\right)\left[-\frac{r}{b_1c_2}\left(\frac{a_1c_2}{r} - u(t)\right)\right] = \Theta(u_k, t), \tag{A4}$$

where $\Theta(u_k, t)$ is defined as in (3.3). Solving (A4) for $u(t)$ can be done by standard algebraic manipulations and the Lambert W function. Equivalently (applying the form $ye^y = \cdot$), one obtains the explicit formula

$$u(t) = u(t, u_k) = \frac{b_1c_2}{r}\,W\left(\Theta(u_k, t)\right) + \frac{a_1c_2}{r}, \tag{A5}$$

for $t \in (kp^+, (k+1)p]$, which is exactly (3.2) with $u_k = \tilde{u}(0^+)$.

When $a_1 = 0$, the flow reduces to $u'(t) = -\dfrac{b_1u}{c_2 + u}$, which again admits a Lambert W representation: for $t \in (kp^+, (k+1)p]$,

$$u(t, u_k) = c_2\,W\left(\frac{u_k}{c_2}\exp\left(\frac{u_k}{c_2} - \frac{b_1(t - kp)}{c_2}\right)\right), \tag{A6}$$

coinciding with (3.5).

Let $\phi(t; u_0)$ be the flow of the equation $u' = a_1 - \dfrac{b_1u}{c_2 + u}$ with $u(0) = u_0 > 0$, then

$$\phi(t; u_0) = u(t, u_0) = \frac{b_1c_2}{r}\,W\left(\Theta(u_0, t)\right) + \frac{a_1c_2}{r}.$$

Define the stroboscopic map

$$P(u_0) := \phi(p; u_0) + \varrho, \qquad u_0 > 0,$$

so that the post-impulse values satisfy $u((k+1)p^+, u_0) = P(u(kp^+))$.

First, we show that the stroboscopic map P is continuous, strictly increasing, and $P(u_0) - u_0$ is strictly decreasing. In fact, the vector field $f_1(u) \triangleq a_1 - \dfrac{b_1u}{c_2 + u}$ is C^1 on $(0, \infty)$, hence $\phi(p; u_0)$ is C^1 in u_0. Moreover, the variational equation gives

$$\frac{\partial\phi(p; u_0)}{\partial u_0} = \exp\left(\int_0^p f'(\phi(s; u_0))\,ds\right), \qquad f_1'(u) = -\frac{b_1c_2}{(c_2 + u)^2} < 0,$$

so $0 < \partial_{u_0}\phi(p; u_0) < 1$ for all $u_0 > 0$. Therefore, $P'(u_0) = \partial_{u_0}\phi(p; u_0) \in (0, 1)$, which implies that P is strictly increasing and that

$$-1 < \frac{d}{du_0}(P(u_0) - u_0) = P'(u_0) - 1 < 0,$$

i.e., $Q(u_0) \triangleq P(u_0) - u_0$ is strictly decreasing on $(0, \infty)$.

Now, we prove the existence and uniqueness of a positive fixed point for the stroboscopic map P. Since $\phi(p; 0^+) \geq 0$ and $\varrho > 0$, we have

$$\lim_{u_0 \to 0^+} Q(u_0) = \lim_{u_0 \to 0^+} (P(u_0) - u_0) = \phi(p; 0^+) + \varrho > 0.$$

On the other hand, since $\lim_{u\to\infty} f_1(u) = -(b_1 - a_1)$, standard comparison implies $\lim_{u_0\to\infty}(\phi(p; u_0) - u_0) = -(b_1 - a_1)p$. Hence $\lim_{u_0\to\infty} Q(u_0) = p - (b_1 - a_1)p < 0$, and therefore $Q(u_0) < 0$ for all sufficiently large u_0. Thus, Q must have at least one zero. Since Q is strictly decreasing, this zero is unique. Denote it by $u^* > 0$, then we have $P(u^*) = u^*$.

In addition, we can further prove that the fixed point is globally asymptotically stable. Let $u_{k+1} = P(u_k)$, $k = 0, 1, 2, \cdots$. Because P is increasing and $Q(u) = P(u) - u$ is strictly decreasing with unique root u^*, we have $Q(u) > 0$ for $u < u^*$ and $Q(u) < 0$ for $u > u^*$. Hence if $u_0 < u^*$, then $u_1 - u_0 = Q(u_0) > 0$, so $\{u_k\}$ is increasing; moreover $u_k < u^*$ for all k (otherwise, by monotonicity, the first crossing would contradict $Q > 0$ below u^*). Thus $\{u_k\}$ is increasing and bounded above by u^*, hence converges to some $\bar{u} \leq u^*$. Passing to the limit in $u_{k+1} = P(u_k)$ gives $\bar{u} = P(\bar{u})$, so $\bar{u} = u^*$. Similarly, if $u_0 > u^*$, then $u_1 - u_0 = Q(u_0) < 0$, so $\{u_k\}$ is decreasing and bounded below by u^*, hence also converges to u^*. Therefore, $u(kp^+) = u_k \to u^* (k \to \infty)$. By continuous dependence of solutions on initial value, the convergence extends to the whole trajectory on each interval $(kp^+, (k + 1)p)$, yielding

$$|u(t) - \tilde{u}(t)| \to 0, \qquad t \to +\infty,$$

where $\tilde{u}(t)$ is the p-periodic solution generated from $\tilde{u}(0^+) = u^*$ and the flow formula (A5). This proves existence, uniqueness, and global stability of the positive p-periodic solution.

Finally, we give the explicit expression for $\tilde{u}(0^+)$. Since $\tilde{u}(p^+) = \tilde{u}(0^+)$, we get $\phi(p; \tilde{u}(0^+)) + \varrho = \tilde{u}(0^+)$. By evaluating the implicit identity (A3) at $t = (k + 1)p$ and imposing $\tilde{u}((k + 1)p^+) = \tilde{u}(kp^+)$, we obtain

$$\tilde{u}(0^+) = \frac{\varrho}{1 - M} + \frac{a_1 c_2}{b_1 - a_1}, \qquad M = \exp\left\{\frac{(b_1 - a_1)\left[\varrho - (b_1 - a_1)p\right]}{b_1 c_2}\right\},$$

which is exactly (3.4). Substituting $\tilde{u}(0^+)$ into (A5) yields (3.2).

(iii) Let $a_1 = 0$ and $\varrho < b_1 p$. The existence and global asymptotic stability of periodic solution follow exactly as above. Solving the periodicity condition $\phi(p; u_1^*) = u_1^* - \varrho$ using (A6) gives $u_1^* = \frac{\varrho}{1-\exp\left(\frac{\varrho - b_1 p}{c_2}\right)}$, which is (3.6). The proof is completed.